

# Modeling and Measurements of Ramping Losses in HTS Coils for Pulsed Power Applications of SMES

Ashish Bhardwaj , Senior Member, IEEE, Nagaraju Guvvala , Member, IEEE, Linh N. Nguyen , Chul H. Kim , Senior Member, IEEE, Peter Cheetham , Member, IEEE, Doan N. Nguyen , and Sastry V. Pamidi , Senior Member, IEEE

**Abstract**—Ramping losses in high-temperature superconductor (HTS) based superconducting magnetic energy storage (SMES) coils are modeled using the finite element technique, and the models were experimentally validated using two independent measurement techniques. The target application of the SMES is a coil set of the 100-Tesla high field pulsed magnet system at Los Alamos National Laboratory. The pulse shape and duration used for the measurement were selected based on the needs of the pulsed magnet system. The modeling and measurement methods used are discussed. The purpose of the models and the experimental validation is to enable reliable estimation of losses in full-scale SMES systems needed for the designs of cryogenic systems. The similarities between the ongoing developments of high current HTS cables for compact fusion systems and the proposed SMES are discussed to show the synergy among the applications and as the reason for the author's optimism of high-current HTS SMES technology operating at 20 K or higher temperatures.

**Index Terms**—Double pancake, FEM, HTS, model validation, REBCO, ramping loss measurements, SMES, power conversion system.

## I. INTRODUCTION

THE large current-carrying capability and the absence of electrical resistance make the HTS attractive for many magnet and electrical power applications [1]. Several research efforts have been devoted to the development of HTS-based

energy storage devices [2], fault current limiters [3], high-field magnets [4], and electrical machines [5]. Rare earth barium copper oxide (REBCO) tape is an attractive conductor for high-current cables of high field magnets and electrical power devices due to its high current carrying capacity, excellent mechanical strength, and operation at 20 K and higher [6]. Several REBCO-based high field magnets [7], [8] and electrical power devices [9], [10], [11] have been demonstrated. SMES is attractive for energy storage because it offers both high energy and power densities [2]. Designs and fabrication of HTS SMES systems for frequency and voltage stabilization in power grids have been published [12]. The design concepts SMES based on solenoid and toroidal designs have been reported [13]. SMES for pulsed power applications is attractive to lower the footprint of the energy storage systems and achieve the target efficiency [13], [14], [15]. Achieving the needed power density and pulse shapes from traditional energy storage devices requires extensive power conversion systems, and the overall system efficiency is low. HTS devices experience energy losses when exposed to a time-varying magnetic field and/or current, called ac losses [16]. The ramping losses significantly impact the electrical and cryogenic thermal designs of SMES regarding their cooling demands, operating temperatures, and efficiency. One of the challenges of SMES, when used for pulsed power applications requiring frequent charging and discharging is the extent of ramping losses. SMES encounter losses during charging and discharging events, and the designs must consider the losses when evaluating the capital and operating costs of the cryogenic cooling systems.

SMES systems in pulsed power applications will see fast current ramping, and the ability to estimate the losses for the desired current pulse shapes and durations is critical for successful designs. This paper discusses the target pulsed power application of high field pulsed magnets using SMES as the energy source, the waveforms of the required high current pulses, the use of finite element modeling (FEM), and experimental measurement of the ramping losses in REBCO coils. The focus of the research is to experimentally validate the use of the  $T - A$  formulation on a double pancake (DP) REBCO coil to estimate ramping losses under the pulses relevant to the target high field pulsed magnet application. Most of the published models and measurements of losses in HTS coils are at power frequencies of 50 and 60 Hz for electric utility applications and high frequencies of 400 Hz for superconducting electric machines for aviation [17]. Also, the reported work is on losses under sinusoidal

Manuscript received 2 October 2023; revised 29 November 2023; accepted 5 December 2023. Date of publication 22 January 2024; date of current version 7 February 2024. This work was supported in part by the N S F Cooperative Agreement under Grants DMR-1644779 and DMR-2128556, and the state of Florida, which was performed at the NHMFL-PFF (also known as MPA-MAGLAB) in Los Alamos, NM, and in part by the Office of Naval Research under Grants N00014-21-1-2124 and N00014-22-1-2640. (Corresponding author: Ashish Bhardwaj.)

Ashish Bhardwaj is with the Los Alamos National Laboratory, Los Alamos, NM 87545 USA, also with the FAMU-FSU College of Engineering, Tallahassee, FL 32310 USA, and also with the Center for Advanced Power Systems, Tallahassee, FL 32310 USA (e-mail: ashish@lanl.gov).

Nagaraju Guvvala and Chul H. Kim are with the Center for Advanced Power Systems, Tallahassee, FL 32310 USA (e-mail: nguvvala@caps.fsu.edu; ckim@caps.fsu.edu).

Linh N. Nguyen and Doan N. Nguyen are with the Los Alamos National Laboratory, Los Alamos, NM 87545 USA (e-mail: linh@lanl.gov; doan@lanl.gov).

Peter Cheetham and Sastry V. Pamidi are with the FAMU-FSU College of Engineering, Tallahassee, FL 32310 USA, and also with the Center for Advanced Power Systems, Tallahassee, FL 32310 USA (e-mail: cheetham@caps.fsu.edu; pamidi@eng.famu.fsu.edu).

Color versions of one or more figures in this article are available at <https://doi.org/10.1109/TASC.2024.3356427>.

Digital Object Identifier 10.1109/TASC.2024.3356427

TABLE I  
DOUBLE PANCAKE REBCO COIL PARAMETERS

Parameters	REBCO Coil
Inner radius ( $R_i$ ) (mm)	33
Outer radius ( $R_o$ ) (mm)	43
Height ( $H_{coil}$ ) (mm)	9.1
Number of turns	2 x 50
Tape width ( $H_{tape}$ ) (mm)	4
Tape thickness ( $T_{tape}$ ) (mm) with insulation	0.2
Coil inductance (mH)	1.1
Tape $I_c$ (A)	87
Coil $I_c$ (A)	~50
Tape specification	SCS4050 AP

waveforms. The pulse shapes and equivalent frequencies needed for pulsed magnet applications differ significantly [15], [18], [19], [20]. This work is on the models and measurements of ramp losses at triangular waveforms and low frequencies. The model development and experimental validation will allow its use for the estimation of loss in a full-size SMES to support the designs. The specifications of the DP REBCO coil used in this study are provided in Table I.

## II. FULL-SCALE SMES FOR PULSED POWER APPLICATION

National High Magnetic Field Laboratory's Pulsed Field Facility (NHMFL-PFF) at Los Alamos National Laboratory (LANL) has the world's highest 100-Tesla pulsed field magnet [18], which is powered by 1430 MVA (1200/600 MJ stored/extractable energy) pulsed power generator [14]. The stored energy is supplied to the 100-Tesla magnet through  $7 \times 87$  MVA, 12-pulse rectifier set capable of maintaining 6.4 kV at 20 kA for the pulse duration [19]. Two of the seven rectifier converters are used to power the outsert magnet's innermost coil group (CG-1). Our previous study [15] established that an SMES with 45 MJ stored energy at 30 kA current is suitable for energizing the CG-1. The SMES and power conversion system (PCS) topology described in [15] can deliver and recover the energy to and from the pulsed magnet, similar to the 1430 MVA pulsed power generator. The SMES can support the flat top current and magnetic field for the desired duration as supplied by the existing system. Also, the 45 MJ SMES was shown to support the pulse duration of 200 ms with a flat top of 20 ms without any distortion or deviation from the pulse shape and width produced by the pulsed power system currently in use [15], as shown in Fig. 1. The 45 MJ SMES can support four pulses along with the option of safety energy dump in case of fault on the pulsed magnet without recharge. The 45 MJ storage capacity and 30 kA operating current were selected to replicate the capabilities of the existing power system for powering the 100-Tesla pulsed magnet system.

## III. ESTIMATION OF RAMP LOSSES USING T-A FORMULATION

Fig. 2 shows one quadrant of the DP coil used for the FEM analysis and Fig. 3 shows 50 A triangular pulse used to estimate the losses in the DP coil. As discussed, in the previous section, pulsed loads require a specific pulse pattern. The frequency of the

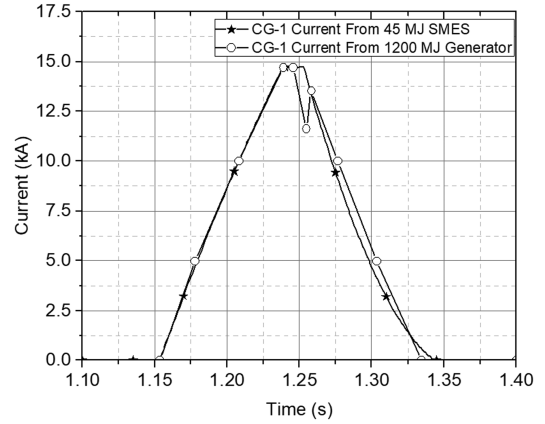


Fig. 1. Operational (Generator) and simulated (SMES) current profile comparison of the CG-1 of the 100 T magnet [15] ©[2023] IEEE.

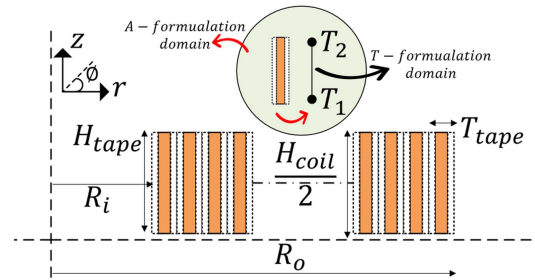


Fig. 2. One quadrant of REBCO double pancake coil.

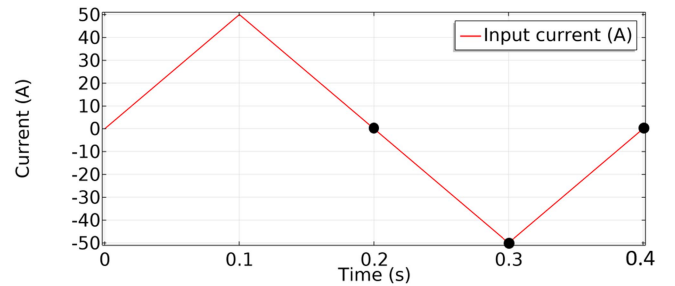


Fig. 3. Applied 50 A triangular current pulse to DP REBCO coil.

current pulse used to match the pulse requirements of the 100-Tesla magnet CG-1 [15]. The  $T - A$  formulation has been used extensively for studying HTS coils due to its fast computation and lower cost [21], [22], [23], [24]. In the mathematical model, the thickness of the REBCO conductors is neglected, and the thin superconducting layer is treated as a 1D line. The sheet current density  $J$  and magnetic flux density  $B$  are solved by applying the state variables  $T$  and  $A$  for the coil [25]. The current in a thin shell can be written as (1) [25], [26].

$$J = \nabla \times T \quad (1)$$

The governing equation of the model is written as (2) [22].

$$\nabla \times (\rho_{hts} \nabla \times T) = -\frac{\partial B}{\partial t} \quad (2)$$

The resistivity of the superconductor is defined by the Kim-Anderson  $E - J$  power as (3) and (4) [22], [25], [27], [28].

$$E = \rho_{hts} \cdot J = \frac{E_c}{J_c(B)} \left| \frac{J}{J_c(B)} \right|^{n(B)-1} \cdot J \quad (3)$$

$$J_c(B) = \frac{J_{c0}}{\left(1 + \frac{\sqrt{k^2 B_{\parallel}^2 + B_{\perp}^2}}{B_c}\right)^b} \quad (4)$$

Here,  $\rho_{hts}$  is the resistivity,  $E_c$  is the critical electric field at  $1 \mu\text{V}/\text{cm}$ ,  $J_c$  is the critical current density,  $J_{c0}$  is the initial critical current density and  $n$  is the superconducting  $n$ -value of the HTS tape.  $B_{\parallel}$  and  $B_{\perp}$  are the parallel and perpendicular components of the magnetic flux density in the HTS tape, respectively. Values 0.25, 0.1 T, and 0.7 were used for the parameters  $k$ ,  $B_c$  and  $b$ , respectively [25], [28]. The total transport current in a tape was calculated by the integration of the current density across the cross-section of the HTS tape as expressed in (5) and reduced to 1D as expressed (6) [25]:

$$I_{hts} = \iint_s J dS = \iint_s \nabla \times T dS = \oint_{\partial S} T dS \quad (5)$$

$$I_{hts} = (T_1 - T_2) t_{hts} \quad (6)$$

where  $I_{hts}$  is transport current flowing in the HTS layer,  $S$  is the cross-section of the tape and  $\partial S$  is the boundary edges of the cross-section.  $T_1$  and  $T_2$  are the current vector potentials at the respective edge points and  $t_{hts}$  is the thickness of HTS layer.

Using the symmetry, simulation was performed in only a quarter of the cross-section of the DP REBCO coil, and the ramp loss estimation was performed for 1.5 cycles of the applied current pulses while the losses in each domain were calculated by spatially integrating  $J \cdot E$  for the second half of the first cycle. If  $S$  is the superconducting domain and  $f$  is the frequency of the applied current, then the losses can be written as in (7) [25].

$$Q = 2 \int_{1/f}^{3/(2f)} \int_S J \cdot E dS dt \quad (7)$$

Figs. 4 and 5 show the ramp losses estimated using the FEM due to triangular and sinusoidal current pulses at different turns in a single pancake of the DP REBCO coil. The behavior of the ramp losses is similar in both type of pulses. When the peak current is low, the losses are higher at the edge turns of the coil, and when peak current gets near  $I_c$  the losses are higher in the middle turns. Though turns of the coil carry the same current, they generate different losses because they experience varying magnetic fields, causing varying magnetization losses. For example, at 50 A peak triangular current pulse as shown in Fig. 6(a)–(c), the magnetic flux  $B_{\perp}$  is higher in the coil's middle turns than the edge turns, generating correspondingly higher losses in the middle section of the coil. Estimating the losses in a coil concerning the transport current is complicated. Generally, the magnetic field profile strongly depends on the current distribution in the coil turns, and the current distribution changes significantly with varying current. Also, the current distribution is expected to change considerably with varying current amplitude. Varying current distribution is the reason for

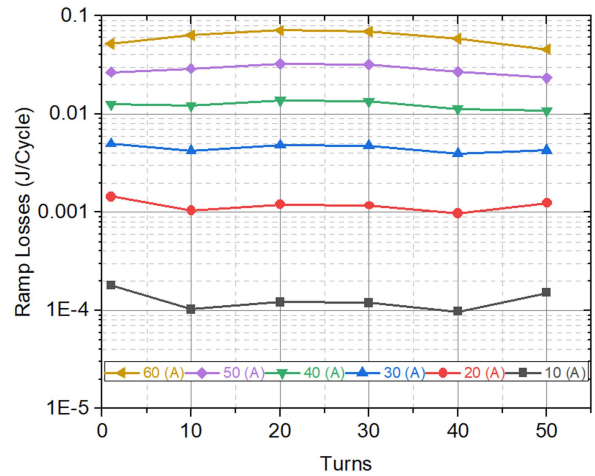


Fig. 4. Ramp losses at different turns for triangular current pulses.

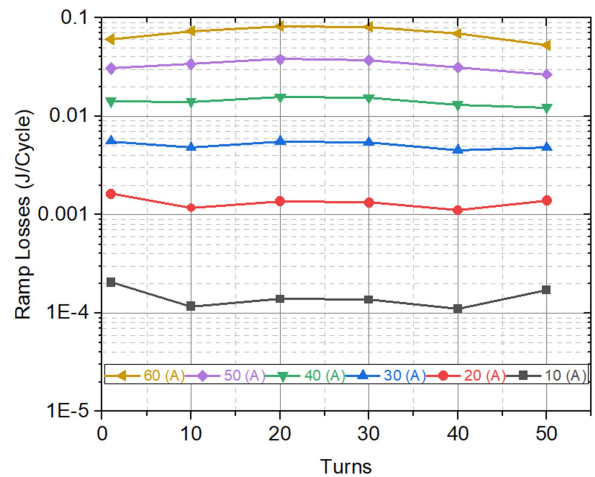


Fig. 5. Ramp losses at different turns for sinusoidal current pulses.

the variation of ramp losses among the turns of the coil when the peak current amplitude changes. In Fig. 6(a)–(c), the magnetic flux  $B_{\perp}$  and the current density show a transition from a positive to a negative value within the same turn at zero crossing and at the peak value of current.

#### IV. EXPERIMENTAL MEASUREMENT OF RAMP LOSSES

The ramping losses in the REBCO coil depend on the size of the coil peak current, frequency, maximum magnetic field, and temperature. The physical mechanisms and scale of the losses in HTS tapes differ for magnetization losses and transport current losses [16], [29], [30].

##### A. Liquid Nitrogen Boil-Off Method

The liquid nitrogen boil-off technique has been used for ac loss measurements in HTS coils [31], [32], [33]. The principle of the ramp loss measurement using the nitrogen boil-off method is as follows:

- 1) The ramping current generates losses in the coil.

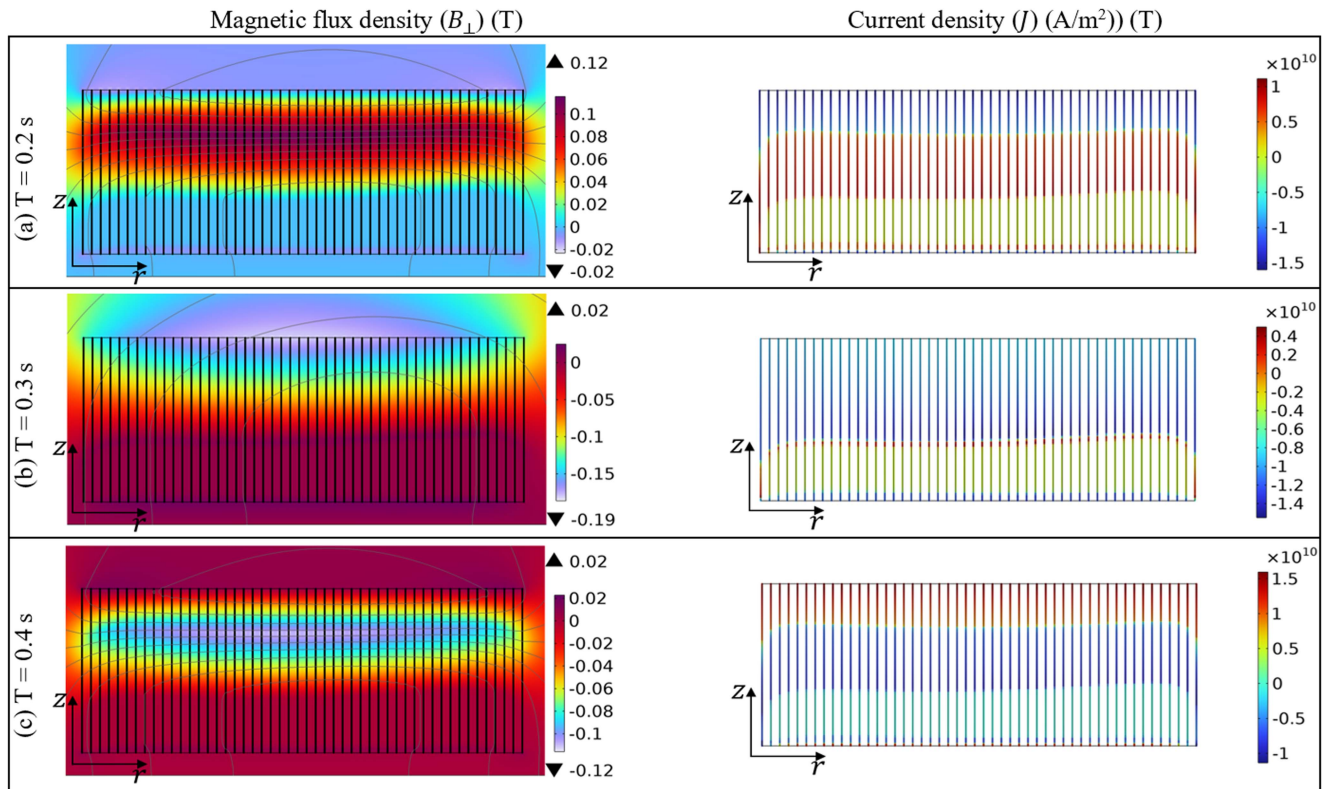


Fig. 6. Magnetic flux and current density distribution in the coil at (a) 0.2 s, (b) 0.3 s, and (c) 0.4 s of triangular current pulse as shown by dots in Fig. 3.

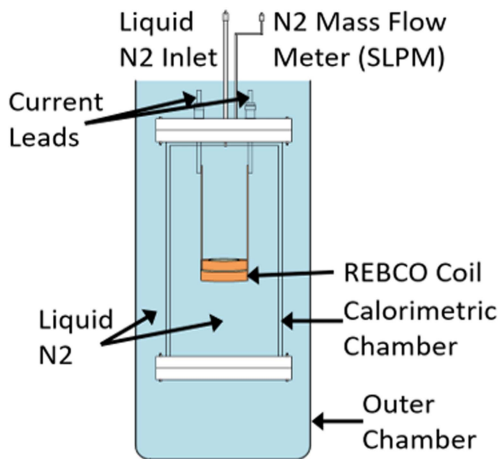


Fig. 7. Simplified schematic of the boil-off loss measurement.

- 2) The heat generated is absorbed by LN<sub>2</sub>, resulting in the evaporation of the corresponding amount of LN<sub>2</sub>.
- 3) Under the equilibrium flow of nitrogen gas, the ramping losses can be calculated from the volume flow rate at room temperature.

Fig. 7 shows the calorimetric chamber used for measuring the nitrogen boil off for the ramping losses. Four main components of the calorimetric setup to measure the ramp losses are a programmable power supply that produces the required current

pulse shape, a current measuring device, a volume flow meter, and a data acquisition (DAQ) system [31]. The coil is housed inside the calorimetric chamber that is filled with LN<sub>2</sub>. The calorimetric chamber including the current lead is immersed completely in the LN<sub>2</sub> bath inside the outer cryostat to minimize the heat leak from outside [31]. A programmable power supply is connected to the current leads of the coil to supply the desired current pulses. A Rogowski coil is used to measure the current through the coil, and a nitrogen gas flow meter was used to measure the volume flow rate. The primary variables are gathered and recorded using the DAQ system.

The ramping losses can be calculated by utilizing the direct relationship between the dissipated heat and the mass flow rate of the gaseous nitrogen. The integrity of the relation between the mass flow rate and the ramp losses was verified using a standard resistive heater up to 45 W. The slope of flow rate versus the heat input line was found to be 0.246 SLPM/W, closely agreeing with the theoretical value of 0.25 SLPM/W [35].

### B. Electrical Method

A second method for measuring the losses was used to serve for future ramping loss measurements at temperatures other than 77 K. The electric method is faster for measuring the losses and is suitable at any temperature and cooling medium. During the ramping of REBCO coils, magnetization losses can occur in superconducting layers because of flux creep and jumps. [36], [37]. It constitutes a major part of ramp losses when supplied with the

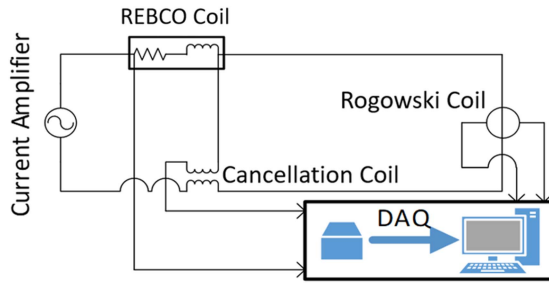


Fig. 8. Schematic of the electrical method for ramp losses measurement.

currents lower than the  $I_c$ , which could lead to a possible quench of the coil [36], [37], [38], [39]. Fig. 8 shows the schematic of the electrical method for loss measurement. The REBCO coil was powered with current from a power amplifier controlled by a signal generator. During the current ramping pulses, REBCO coil develops two voltages, one in resistive  $R_{HTS}$  part ( $V_R$ ) and another in the inductive  $L_{HTS}$  part ( $V_L$ ) and they can be expressed as (8). The cancellation coil is designed to cancel the inductive part of the induced voltage. If the mutual inductance of the cancellation coil is,  $M_{Comp}$  then compensated voltage can be expressed as (9).

$$V_{Coil} = V_R + V_L = R_{HTS}I + L_{HTS}\dot{I} \quad (8)$$

$$V_{Comp} = M_{Comp}\dot{I} = V_L \quad (9)$$

Thus, to get the resistive component  $L_{HTS}$  should be equal to  $M_{Comp}$ . If the diameters of the primary and the secondary windings of the cancellation system setup are  $D_{pri}$  and  $D_{sec}$ , respectively and the number of turns in the primary winding of the cancelling coil are  $N_{pri}$  then the minimum required number of turns in the secondary winding ( $N_{sec}$ ) of the cancelling coil can be calculated from the (10), assuming perfect flux linkage between the primary and secondary windings of the coil.

$$N_{sec} = \left( \frac{4}{\mu_0\pi} \cdot \frac{D_{pri}}{D_{sec}^2} \right) \cdot L_{HTS} \quad (10)$$

The voltage taps of the REBCO coil was connected in anti-series with the voltage taps from the cancellation coil to compensate the inductive component [28], [31], [32]. The magnitude of the cancellation voltage was adjusted to minimize the phase difference between the input current (to the REBCO coil) and the voltage signal from the REBCO coil after removing the voltage induced by the cancellation coil. The resulting voltage is the resistive component and can be recorded as the ramp loss voltage [31]. The ramp losses can be calculated in (J/cycle) using (11) [32].

$$Q = \frac{V_{rms} \cdot I_{rms}}{f} \quad (11)$$

where  $f$  is frequency of the ramping current and  $V_{rms}$  and  $I_{rms}$  are the RMS values of the compensated voltage and the current in the REBCO coil, respectively. Figs. 9 and 10 show an example of the results of boil-off and electrical loss measurement methods, respectively.

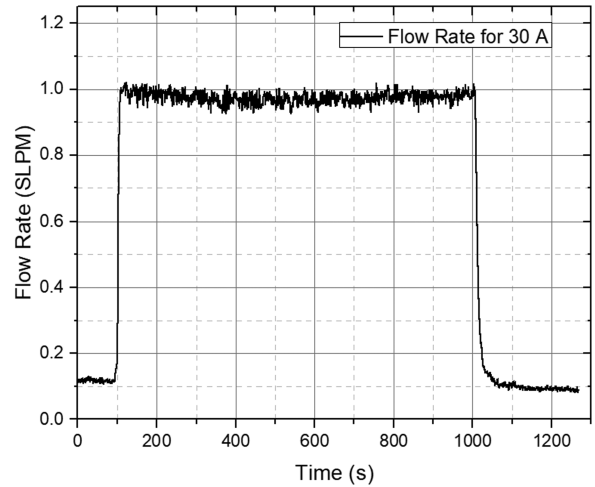


Fig. 9. Example of measured flowrate by boil-off method.

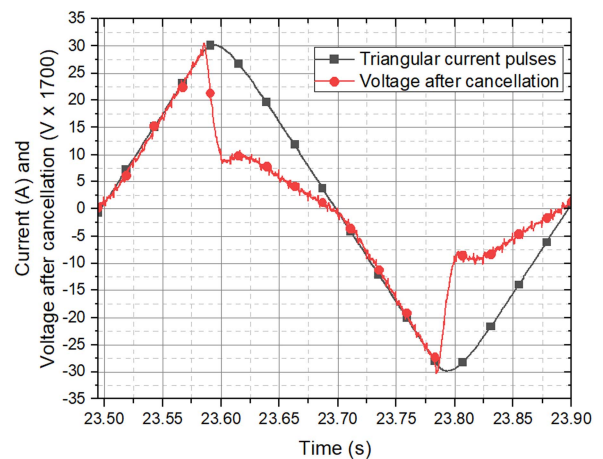


Fig. 10. Example of measured current and voltage by electrical method.

## V. EXPERIMENTAL RESULTS

The power amplifier was used for generating triangular and sinusoidal current pulses for DP REBCO coil. The current amplitude ranged from 10 A to 40 A, peak. It is challenging to use lock-in amplifier method to measure the ramp losses for triangular current pulses [40]. Ramp losses of the coil were measured at 2.5 Hz and 60 Hz. No distinguishable differences were found in the results of calorimetric and electrical methods. It was observed that the ramp losses per cycle were independent of frequency for the 2–60 Hz range. This indicates that the measured losses were mainly hysteretic losses. Figs. 11 and 12 show the measured the ramping losses.

The measured ramping losses (J/cycle) at each frequency are consistent as expected for hysteretic losses. The magnitude of the losses independently obtained from two experimental methods are in good agreement with the values predicted from the FEM. The measurement of the ramp losses was limited to 40 A to avoid the quench of the coil. Table II shows the error in the losses between simulation and the two measurement methods for triangular current pulses.

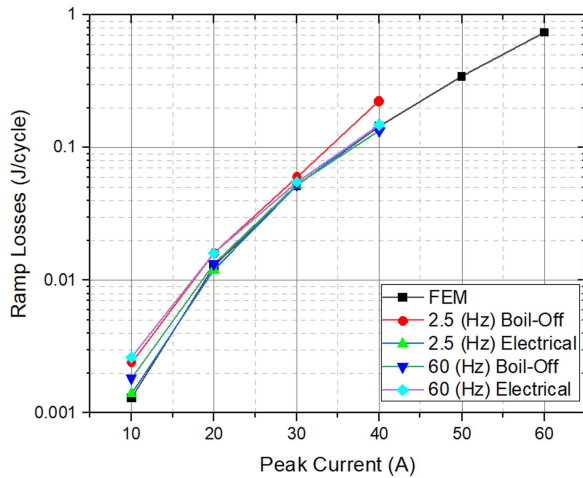


Fig. 11. Ramp losses for triangular current pulses in DP REBCO coil.

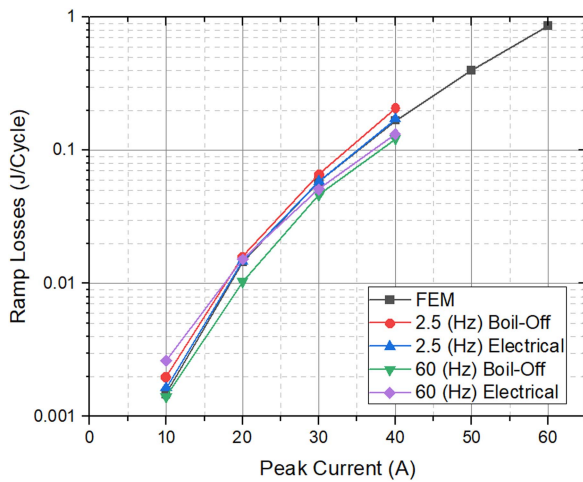


Fig. 12. Ramp losses for sinusoidal current pulses in DP REBCO coil.

TABLE II  
% ERROR (SIMULATION AND MEASUREMENTS)

Current	Simulation and Boil Off	Simulation and Electrical
10 A	5.15	10.60
20 A	0.91	5.12
30 A	0.64	2.21
40 A	4.26	1.01

## VI. DISCUSSION

The full-scale SMES discussed in Section II is at 45 MJ and 30 kA. High field magnets (up to 20 T) using high current (up to 50 kA) HTS cables are an active development area [41], [42], [43]. Compact fusion systems development activities are building REBCO magnet systems for 20 K operation. The compact fusion magnet development will benefit SMES because of the similarities of challenges, including high current, high strength cables, the need for ac loss reduction, and the need for high efficiency cryogenic systems operating at or above 20 K [44], [45], [46]. The synergy with the high field magnets and the validated designs for high current cables and 20 K cryogenic

cooling schemes using forced flow gaseous helium circulation will facilitate SMES development [44], [45], [46], [47], [48], [49].

## VII. CONCLUSION

Ramping loss estimation of REBCO coil was performed for sine and triangular waveforms using FEM, using the  $T - A$  formulation, and the modeled results were compared with the experimental data obtained using two independent measurement techniques, an electrical method suitable for any temperature and cooling media and the liquid nitrogen boil-off calorimetric method suitable for 77 K, liquid nitrogen cooled systems.

The validity of the two measurement methods for ramping losses under the pulse shapes needed for the target pulsed magnet application was demonstrated. The agreement of the experimental and modeled ramping losses will enable the use of the model for calculating the losses for full-scale SMES. Future studies will focus on the loss estimation in full-scale SMES to generate the data necessary for designing the cryogenic systems. Future studies will also include measuring and modeling ramping losses in high current cables necessary for building the 45 MJ SMES needed for pulsed magnets at LANL.

## REFERENCES

- [1] C. R. Vargas-Llanos, J. Krämer, M. Noë, and F. Grilli, "Design and test of a setup for calorimetric measurements of AC transport losses in HTS racetrack coils," *Supercond. Sci. Technol.*, vol. 36, no. 4, Mar. 2023, Art. no. 045015, doi: [10.1088/1361-6668/acbba5](https://doi.org/10.1088/1361-6668/acbba5).
- [2] C. C. Rong and P. N. Barnes, "Developmental challenges of SMES Technology for applications," *IOP Conf. Ser.: Mater. Sci. Eng.*, vol. 279, Dec. 2017, Art. no. 012013, doi: [10.1088/1757-899x/279/1/012013](https://doi.org/10.1088/1757-899x/279/1/012013).
- [3] M. R. Barzegar-Bafrooei, A. A. Foroud, J. D. Ashkezari, and M. Niasati, "On the advance of SFCL: A comprehensive review," *IET Gener., Transmiss. Distrib.*, vol. 13, no. 17, pp. 3745–3759, Aug. 2019, doi: [10.1049/iet-gtd.2018.6842](https://doi.org/10.1049/iet-gtd.2018.6842).
- [4] H. Maeda and Y. Yanagisawa, "Recent developments in high-temperature superconducting magnet technology (review)," *IEEE Trans. Appl. Supercond.*, vol. 24, no. 3, Jun. 2014, Art. no. 4602412, doi: [10.1109/TASC.2013.2287707](https://doi.org/10.1109/TASC.2013.2287707).
- [5] K. S. Haran et al., "High power density superconducting rotating machines—Development status and technology roadmap," *Supercond. Sci. Technol.*, vol. 30, no. 12, Nov. 2017, Art. no. 123002, doi: [10.1088/1361-6668/aa833e](https://doi.org/10.1088/1361-6668/aa833e).
- [6] C. Barth, G. Mondonico, and C. Senatore, "Electro-mechanical properties of REBCO coated conductors from various industrial manufacturers at 77 K, self-field and 4.2 K, 19 T," *Supercond. Sci. Technol.*, vol. 28, no. 4, Feb. 2015, Art. no. 045011, doi: [10.1088/0953-2048/28/4/045011](https://doi.org/10.1088/0953-2048/28/4/045011).
- [7] S. Hahn et al., "45.5-tesla direct-current magnetic field generated with a high-temperature superconducting magnet," *Nature*, vol. 570, no. 7762, pp. 496–499, Jun. 2019, doi: [10.1038/s41586-019-1293-1](https://doi.org/10.1038/s41586-019-1293-1).
- [8] M. Paidpilli and V. Selvamaniackam, "Development of RE-Ba-Cu-O superconductors in the U.S. for ultra-high field magnets," *Supercond. Sci. Technol.*, vol. 35, no. 4, Feb. 2022, Art. no. 043001, doi: [10.1088/1361-6668/ac5162](https://doi.org/10.1088/1361-6668/ac5162).
- [9] Y. Ohtsubo et al., "Development of REBCO superconducting transformers with a current limiting function—Fabrication and tests of 6.9 kV-400 kVA transformers," *IEEE Trans. Appl. Supercond.*, vol. 25, no. 3, Jun. 2015, Art. no. 5500305, doi: [10.1109/TASC.2014.2374671](https://doi.org/10.1109/TASC.2014.2374671).
- [10] H. Sasa et al., "Experimental evaluation of 1 kW-class prototype REBCO fully superconducting synchronous motor cooled by subcooled liquid nitrogen for E-aircraft," *IEEE Trans. Appl. Supercond.*, vol. 31, no. 5, Aug. 2021, Art. no. 5200706, doi: [10.1109/TASC.2021.3055452](https://doi.org/10.1109/TASC.2021.3055452).
- [11] W. H. Fietz, M. J. Wolf, A. Preuss, R. Heller, and K.-P. Weiss, "High-current HTS cables: Status and actual development," *IEEE Trans. Appl. Supercond.*, vol. 26, no. 4, Jun. 2016, Art. no. 4800705, doi: [10.1109/TASC.2016.2517319](https://doi.org/10.1109/TASC.2016.2517319).

- [12] D. Sutanto and K. W. E. Cheng, "Superconducting magnetic energy storage systems for power system applications," in *Proc. IEEE Int. Conf. Appl. Supercond. Electromagn. Devices*, 2009, pp. 377–380, doi: [10.1109/ASEMD.2009.5306614](https://doi.org/10.1109/ASEMD.2009.5306614).
- [13] A. Morandi, M. Fabbri, B. Gholizad, F. Grilli, F. Sirois, and V. M. R. Zermeño, "Design and comparison of a 1-MW/5-s HTS SMES with toroidal and solenoidal geometry," *IEEE Trans. Appl. Supercond.*, vol. 26, no. 4, Jun. 2016, Art. no. 5700606, doi: [10.1109/TASC.2016.2535271](https://doi.org/10.1109/TASC.2016.2535271).
- [14] H. J. Boenig, J. B. Schillig, H. E. Konkel, P. L. Klingner, T. L. Petersen, and J. D. Rogers, "Design installation and commissioning of the Los Alamos National Laboratory pulsed power generator," *IEEE Trans. Energy Convers.*, vol. 7, no. 2, pp. 260–266, Jun. 1992, doi: [10.1109/60.136219](https://doi.org/10.1109/60.136219).
- [15] A. Bhardwaj et al., "Superconducting magnetic energy storage for pulsed power magnet applications," *IEEE Trans. Appl. Supercond.*, vol. 33, no. 5, Aug. 2023, Art. no. 5700306, doi: [10.1109/TASC.2023.3265620](https://doi.org/10.1109/TASC.2023.3265620).
- [16] F. Grilli, E. Pardo, A. Stenvall, D. N. Nguyen, W. Yuan, and F. Gömöry, "Computation of losses in HTS under the action of varying magnetic fields and currents," *IEEE Trans. Appl. Supercond.*, vol. 24, no. 1, Feb. 2014, Art. no. 8200433, doi: [10.1109/TASC.2013.2259827](https://doi.org/10.1109/TASC.2013.2259827).
- [17] K. Kails et al., "Loss characteristics of HTS coated conductors in field windings of electric aircraft propulsion motors," *Supercond. Sci. Technol.*, vol. 33, 2020, Art. no. 064006, doi: [10.1088/1361-6668/ab89ed](https://doi.org/10.1088/1361-6668/ab89ed).
- [18] D. N. Nguyen, J. Michel, and C. H. Mielke, "Status and development of pulsed magnets at the NHMFL pulsed field facility," *IEEE Trans. Appl. Supercond.*, vol. 26, no. 4, Jun. 2016, Art. no. 4300905, doi: [10.1109/TASC.2016.2515982](https://doi.org/10.1109/TASC.2016.2515982).
- [19] J. Sims et al., "First 100 T non-destructive magnet," *IEEE Trans. Appl. Supercond.*, vol. 10, no. 1, pp. 510–513, Mar. 2000, doi: [10.1109/77.828284](https://doi.org/10.1109/77.828284).
- [20] J. Schillig et al., "Operating experience of the United States national high magnetic field laboratory 60 T long pulse magnet," *IEEE Trans. Appl. Supercond.*, vol. 10, no. 1, pp. 526–529, Mar. 2000, doi: [10.1109/77.828288](https://doi.org/10.1109/77.828288).
- [21] H. Zhang, M. Zhang, and W. Yuan, "An efficient 3D finite element method model based on the T-A formulation for superconducting coated conductors," *Supercond. Sci. Technol.*, vol. 30, no. 2, Feb. 2017, Art. no. 024005, doi: [10.1088/1361-6668/30/2/024005](https://doi.org/10.1088/1361-6668/30/2/024005).
- [22] F. Liang et al., "A finite element model for simulating second generation high temperature superconducting coils/stacks with large number of turns," *J. Appl. Phys.*, vol. 122, no. 4, Jul. 2017, Art. no. 043903, doi: [10.1063/1.4995802](https://doi.org/10.1063/1.4995802).
- [23] T. Benkel et al., "T-A formulation to model electrical machines with HTS coated conductor coils," *IEEE Trans. Appl. Supercond.*, vol. 30, no. 6, Sep. 2020, Art. no. 5205807, doi: [10.1109/TASC.2020.2968950](https://doi.org/10.1109/TASC.2020.2968950).
- [24] E. Berrospe-Juarez, F. Trillaud, V. M. R. Zermeño, F. Grilli, H. W. Weijers, and M. D. Bird, "Screening currents and hysteresis losses in the REBCO insert of the 32 T all-superconducting magnet using T-A homogenous model," *IEEE Trans. Appl. Supercond.*, vol. 30, no. 4, Jun. 2020, Art. no. 4600705, doi: [10.1109/TASC.2020.2969865](https://doi.org/10.1109/TASC.2020.2969865).
- [25] L. N. Nguyen, N. Shields, S. Ashworth, and D. N. Nguyen, "Understanding ac losses in CORC cables of YBCO superconducting tapes by numerical simulations," *J. Appl. Phys.*, vol. 134, no. 14, Oct. 2023, Art. no. 143903, doi: [10.1063/5.0162439](https://doi.org/10.1063/5.0162439).
- [26] Y. Yang, H. Yong, X. Zhang, and Y. Zhou, "Numerical simulation of superconducting generator based on the T-A formulation," *IEEE Trans. Appl. Supercond.*, vol. 30, no. 8, Dec. 2020, Art. no. 5207611, doi: [10.1109/TASC.2020.3005503](https://doi.org/10.1109/TASC.2020.3005503).
- [27] F. Huber, W. Song, M. Zhang, and F. Grilli, "The T-A formulation: An efficient approach to model the macroscopic electromagnetic behaviour of HTS coated conductor applications," *Supercond. Sci. Technol.*, vol. 35, no. 4, Mar. 2022, Art. no. 043003, doi: [10.1088/1361-6668/ac5163](https://doi.org/10.1088/1361-6668/ac5163).
- [28] J. Yang et al., "Analysis of AC transport loss in conductor on round core cables," *J. Supercond. Novel Magnetism*, vol. 35, no. 1, pp. 57–63, Sep. 2022, doi: [10.1007/s10948-021-06031-5](https://doi.org/10.1007/s10948-021-06031-5).
- [29] H. Zhang, P. Machura, K. Kails, H. Chen, and M. Mueller, "Dynamic loss and magnetization loss of HTS coated conductors, stacks, and coils for high-speed synchronous machines," *Supercond. Sci. Technol.*, vol. 33, no. 8, Jul. 2020, Art. no. 084008, doi: [10.1088/1361-6668/ab9ace](https://doi.org/10.1088/1361-6668/ab9ace).
- [30] M. Yazdani-Asrami, W. Song, M. Zhang, W. Yuan, and X. Pei, "Magnetization loss in HTS coated conductor exposed to harmonic external magnetic fields for superconducting rotating machine applications," *IEEE Access*, vol. 9, pp. 77930–77937, 2021, doi: [10.1109/ACCESS.2021.3062278](https://doi.org/10.1109/ACCESS.2021.3062278).
- [31] J.-H. Kim, C. H. Kim, G. Iyyani, J. Kvitkovic, and S. Pamidi, "Transport AC loss measurements in superconducting coils," *IEEE Trans. Appl. Supercond.*, vol. 21, no. 3, pp. 3269–3272, Jun. 2011, doi: [10.1109/TASC.2010.2089485](https://doi.org/10.1109/TASC.2010.2089485).
- [32] W. Yuan, T. Coombs, J. N. Kim, C. S. Kim, J. Kvitkovic, and S. Pamidi, "Measurements and calculations of transport AC loss in second generation high temperature superconducting pancake coils," *J. Appl. Phys.*, vol. 110, no. 11, Dec. 2011, Art. no. 113906, doi: [10.1063/1.3662174](https://doi.org/10.1063/1.3662174).
- [33] H. Okamoto, F. Sumiyoshi, K. Miyoshi, and Y. Suzuki, "The nitrogen boil-off method for measuring AC losses in HTS coils," *IEEE Trans. Appl. Supercond.*, vol. 16, no. 2, pp. 105–107, Jun. 2006, doi: [10.1109/TASC.2005.869557](https://doi.org/10.1109/TASC.2005.869557).
- [34] Y. S. Wang, X. J. Guan, and J. Shu, "Review of AC loss measuring methods for HTS tape and unit," in *Proc. IEEE Int. Conf. Appl. Supercond. Electromagn. Devices*, 2013, pp. 560–566, doi: [10.1109/ASEMD.2013.6780846](https://doi.org/10.1109/ASEMD.2013.6780846).
- [35] J. Ekin, *Experimental Techniques: Cryostat Design, Material Properties and Superconductor Critical-Current Testing*. London, U.K.: Oxford Univ. Press, 2006.
- [36] Y. Wang, H. Bai, J. Li, M. Zhang, and W. Yuan, "Electromagnetic modelling using T-A formulation for high-temperature superconductor (RE)Ba<sub>2</sub>Cu<sub>3</sub>O<sub>x</sub> high field magnets," *High Voltage*, vol. 5, no. 2, pp. 218–226, Apr. 2020, doi: [10.1049/hve.2019.0120](https://doi.org/10.1049/hve.2019.0120).
- [37] Z. Jiang et al., "The dynamic resistance of YBCO coated conductor wire: Effect of DC current magnitude and applied field orientation," *Supercond. Sci. Technol.*, vol. 31, no. 3, Jan. 2018, Art. no. 035002, doi: [10.1088/1361-6668/aaa49e](https://doi.org/10.1088/1361-6668/aaa49e).
- [38] E. Berrospe-Juarez, V. M. Zermeño, F. Trillaud, and F. Grilli, "Iterative multi-scale method for estimation of hysteresis losses and current density in large-scale HTS systems," *Supercond. Sci. Technol.*, vol. 31, no. 9, Jul. 2018, Art. no. 095002, doi: [10.1088/1361-6668/aad224](https://doi.org/10.1088/1361-6668/aad224).
- [39] J. Lu, E. S. Choi, H. Kandel, D. V. Abramov, and W. D. Markiewicz, "Hysteresis loss of REBCO conductor up to 35 T," *IEEE Trans. Appl. Supercond.*, vol. 24, no. 3, Jun. 2014, Art. no. 8200104, doi: [10.1109/TASC.2013.2281022](https://doi.org/10.1109/TASC.2013.2281022).
- [40] K. Zhu et al., "AC loss measurement of HTS coil under periodic current," *Physica C: Supercond. Appl.*, vol. 569, Feb. 2020, Art. no. 1353562, doi: [10.1016/j.physc.2019.1353562](https://doi.org/10.1016/j.physc.2019.1353562).
- [41] V. Fry, A. Cecchini, P. Michael, E. Salazar, R. M. Vieira, and Z. S. Hartwig, "Simultaneous transverse loading and axial strain for REBCO cable tests in the SULTAN facility," *Supercond. Sci. Technol.*, vol. 35, Apr. 2022, Art. no. 075007, doi: [10.1088/1361-6668/ac6bcc](https://doi.org/10.1088/1361-6668/ac6bcc).
- [42] Z. S. Hartwig et al., "VIPER: An industrially scalable high-current high-temperature superconductor cable," *Supercond. Sci. Technol.*, vol. 33, no. 11, Oct. 2020, Art. no. 11LT01, doi: [10.1088/1361-6668/abb8c0](https://doi.org/10.1088/1361-6668/abb8c0).
- [43] T. Mulder et al., "Design and manufacturing of a 45 kA at 10 T REBCO-CORC cable-in-conduit conductor for large-scale magnets," *IEEE Trans. Appl. Supercond.*, vol. 26, no. 4, Jun. 2016, Art. no. 4803605, doi: [10.1109/TASC.2016.2527241](https://doi.org/10.1109/TASC.2016.2527241).
- [44] H. Vaghela, V. J. Lakhera, and B. Sarkar, "Forced flow cryogenic cooling in fusion devices: A review," *Heliyon*, vol. 7, no. 1, Jan. 2021, Art. no. e06053, doi: [10.1016/j.heliyon.2021.e06053](https://doi.org/10.1016/j.heliyon.2021.e06053).
- [45] D. Henry et al., "Process flow and functional analysis of the ITER cryogenic system," *AIP Conf. Proc.*, vol. 1218, no. 1, pp. 676–683, Apr. 2010.
- [46] C. Hoa et al., "Installation and pre-commissioning of the cryogenic system of JT-60SA Tokamak," *IOP Conf. Ser.: Mater. Sci. Eng.*, vol. 171, Feb. 2017, Art. no. 012047, doi: [10.1088/1757-899x/171/1/012047](https://doi.org/10.1088/1757-899x/171/1/012047).
- [47] F. Michel et al., "Cryogenic requirements for the JT-60SA Tokamak," *AIP Conf. Proc.*, vol. 1434, no. 1, pp. 78–85, Jun. 2012, doi: [10.1063/1.4706907](https://doi.org/10.1063/1.4706907).
- [48] S. Pamidi, C. H. Kim, J.-H. Kim, D. Crook, and S. Dale, "Cryogenic helium gas circulation system for advanced characterization of superconducting cables and other devices," *Cryogenics*, vol. 52, no. 4–6, pp. 315–320, Apr. 2012, doi: [10.1016/j.cryogenics.2011.09.006](https://doi.org/10.1016/j.cryogenics.2011.09.006).
- [49] C. H. Kim, S.-K. Kim, L. Graber, and S. V. Pamidi, "Cryogenic thermal studies on terminations for helium gas cooled superconducting cables," *Phys. Procedia*, vol. 67, pp. 201–207, 2015, doi: [10.1016/j.phpro.2015.06.035](https://doi.org/10.1016/j.phpro.2015.06.035).